

Modeling acoustic agitation for enhanced development of PMMA resists

R. H. Nilson, S. K. Griffiths, A. Ting

Abstract Although acoustic agitation is known to enhance the development rate of LIGA resists, the operative physical mechanism is not well understood. Analytical and numerical models presented here suggest that the observed enhancement results from steady acoustic streaming and associated polymer fragment transport induced by the high frequency sound waves. The computed steady flow within the feature is torroidal with downflow along the feature walls and upflow in the center. The numerically calculated enhancement of fragment transport is shown to be well approximated by a closed-form expression based on a pair of asymptotic formulas for weak and strong agitation. These transport models are combined with a model of PMMA dissolution kinetics and used to predict development rates for a range of LIGA feature sizes. The results are in good agreement with experimental data from Forschungszentrum Karlsruhe.

1 Introduction

LIGA is a multistep process used to manufacture high-resolution, high aspect-ratio microdevices having micron to millimeter features [1]. A high-energy X-ray source is used to expose a thick photoresist, typically PMMA, through a lithographically produced mask. The exposed material is then removed by chemical dissolution in a development bath to produce a nonconducting mold having deep cavities that are subsequently filled by means of electrodeposition.

The development of exposed PMMA resists can be difficult and time-consuming when the resist thickness is large (~ 1 mm) and feature aspect ratios exceed about four. This is due mainly to limitations on the development rate imposed by transport of PMMA fragments away from

the dissolution surface. Bath stirring enhances transport in features having low aspect ratios, but the fluid in the bottom of high aspect-ratio features remains nearly stagnant, such that transport occurs by diffusion alone [2]. With increasing feature depth, the path length for diffusion becomes progressively longer, reducing the rate of transport and increasing the required development time. In addition, the dependence of transport on aspect ratio may lead to faster development of wide features relative to narrow ones, causing undercutting along the PMMA/substrate interface adjacent to wider features.

Acoustic agitation offers a promising means for enhancing transport rates within high aspect ratio features. A number of researchers have demonstrated experimentally that development rates can be increased several fold by performing the process in acoustic baths like those used for cleaning semiconductor wafers [3, 4]. However, the physical mechanism of this enhancement is not well understood. Although acoustic bubbles may be important in some applications [5], the acoustic power levels of $< 100 \text{ kW/m}^2$ (10 W/cm^2) used in LIGA are below the threshold required to produce cavitation at megasonic frequencies [6].

The present paper demonstrates that the observed acoustic enhancement of LIGA development rates can be attributed to acoustic streaming within features. In this mechanism, the steady streaming flow induced by high frequency agitation circulates most of the fluid within features, substantially increasing polymer fragment transport. The induced flow and fragment transport are computed by numerically solving the governing Navier–Stokes and species transport equations. These numerical results are used to guide the derivation of closed-form analytical expressions for the enhanced transport resulting from any choice of process parameters.

To simulate the coupled processes of PMMA dissolution and fragment transport, the derived analytical expression for fragment transport is combined with a semi-empirical model of polymer dissolution kinetics that includes the effects of temperature and local X-ray dose. Predictions of this coupled model are compared with experimental data reported by Zanghellini et al. [3] for a range of feature sizes, acoustic intensities, and exposure conditions.

2 Governing equations

To model the effects of acoustic agitation in recessed features we consider the simplified geometry of a single trench-like feature of depth h and width w . The fluid

Received: 10 August 2001/Accepted: 24 September 2001

R. H. Nilson (✉), S. K. Griffiths, A. Ting
Sandia National Laboratories,
Livermore, California 94551-0969, USA

This work was supported by the Sandia Materials Science Research Foundation and by the Accelerated Strategic Computing Initiative. Sandia is a multiprogram laboratory operated by Sandia Corporation for the United States Department of Energy under contract DE-AC04-94AL85000.

This paper was presented at the Fourth International Workshop on High Aspect Ratio Microstructure Technology HARMST 2001 in June 2001.

velocity field within the feature is obtained by solving the Navier–Stokes equations using a method of successive approximations that splits the solution into sinusoidal and steady components [7, 8]. The pressure, p , density, ρ , and velocity $\mathbf{u} = u\mathbf{i} + v\mathbf{j}$ are each written as an infinite series.

$$\begin{aligned} p &= p_0 + p_a + p_s + \cdots & \rho &= \rho_0 + \rho_a + \rho_s + \cdots \\ \mathbf{u} &= \mathbf{u}_a + \mathbf{u}_s + \cdots \end{aligned} \quad (1)$$

The ambient values of pressure and density, p_0 and ρ_0 , are taken as constant and uniform. The acoustic terms, subscripted a, are harmonic functions of time but may vary arbitrarily with position. The steady acoustic streaming terms, subscripted s, are time invariant but are free to vary spatially. These series expansions are substituted into the Navier–Stokes equations and terms of like time dependence are equated. The first-order harmonic terms and their products with p_0 and ρ_0 yield the linearized acoustic equations [7, 8] which are solved by superposing exact solutions derived by Rayleigh [7].

The equations governing the steady acoustic streaming flow are deduced by taking the time average of the series expansion of the Navier–Stokes equations. The averaging process eliminates all of the simple harmonic terms but leaves the steady flow quantities, subscripted s below, as well as the time averaged products of harmonic functions that are gathered into \mathbf{F} .

$$\nabla \cdot \mathbf{u}_s = 0 \quad \nabla p_s - \mu \nabla^2 \mathbf{u}_s = \mathbf{F} \quad (2)$$

$$\mathbf{F} = -\rho_0 \langle (\mathbf{u}_a \cdot \nabla) \mathbf{u}_a + \mathbf{u}_a (\nabla \cdot \mathbf{u}_a) \rangle \quad (3)$$

The steady streaming motion is driven by an apparent body force, \mathbf{F} , arising from the Reynolds stresses produced by the harmonic motion. The steady velocity field is used to solve the conservation equation describing steady diffusive and advective transport of a single species.

$$\nabla \cdot (\mathbf{u}_s C) = \nabla \cdot (D \nabla C) \quad (4)$$

C and D are the fragment concentration and diffusivity.

3

Harmonic velocity field

Rayleigh derived traveling wave solutions that satisfy the two-dimensional Cartesian form of the acoustic wave equations for a channel bounded by infinite parallel planes [7]. Because of the nonslip condition on the bounding walls, thin viscous boundary layers of uniform thickness develop interior to the feature along the feature side walls.

The formulas given below can be used to calculate the amplitude of the motion at the feature mouth, u_{a0} , acoustic boundary layer thickness, δ , and wave length, λ .

$$u_{a0} = \sqrt{\frac{I}{\rho c}} \approx 0.2 \text{ m/s} \quad \delta = \sqrt{\frac{2\mu}{\omega \rho}} \approx 0.6 \mu\text{m} \quad (5)$$

$$\lambda = \frac{c}{f} \approx 1.5 \text{ mm} \quad (6)$$

The above numerical estimates are based on a frequency, $f = \omega/2\pi = 1 \text{ MHz}$, and a sound intensity, $I = 60 \text{ kW/m}^2$ (6 W/cm^2), typical of commercial wafer cleaning baths, and fluid properties like those of water: $\rho = 1000 \text{ kg/m}^3$, $c = 1500 \text{ m/s}$ and $\mu = 10^{-3} \text{ Pa s}$.

The Rayleigh solution indicates that the amplitude of the acoustic wave will not be attenuated by more than 20% within the feature provided that $w/\delta > 4$ and $\pi h \delta / \lambda w < 0.2$. These criteria are both met by features having a width of at least $10 \mu\text{m}$ and a depth no greater than 1 mm . Thus, wave attenuation is of little concern in most LIGA applications.

4

Steady streaming and transport

Numerical methods are used to compute the steady fluid flow and associated transport of polymer fragments induced by acoustic agitation. The Navier–Stokes Eqs. (2) and (3) governing the streaming motion are rewritten in terms of the stream function and vorticity, as appropriate for steady incompressible flows [2]. The Reynolds stresses, denoted \mathbf{F} , are evaluated by substitution of the Rayleigh acoustic solutions into Eq. (3). These equations and the species transport equation, Eq. (4), are discretized using second-order finite differences to obtain a system of algebraic equations that are solved iteratively on a rectangular mesh.

After scaling of the position coordinates and fluid velocities by w and D/w , the governing equations contain only three dimensionless parameters, the Peclet Number, aspect ratio, and normalized thickness of the acoustic boundary layer.

$$\text{Pe}_w = \frac{u_{s0} w}{D} \quad A = \frac{h}{w} \quad \delta^* = \frac{\delta}{w} \quad (7)$$

The Peclet number, Pe_w , indicates the relative strength of convective transport by acoustic streaming compared to transport by diffusion. It is based upon a nominal acoustic streaming speed of

$$u_{s0} \equiv \frac{u_{a0}^2}{c} = \frac{I}{\rho c^2} \approx 27 \mu\text{m/sec} \quad (8)$$

The numerical estimate given above corresponds to an acoustic intensity of $I = 60 \text{ kW/m}^2$ (6 W/cm^2) in a fluid

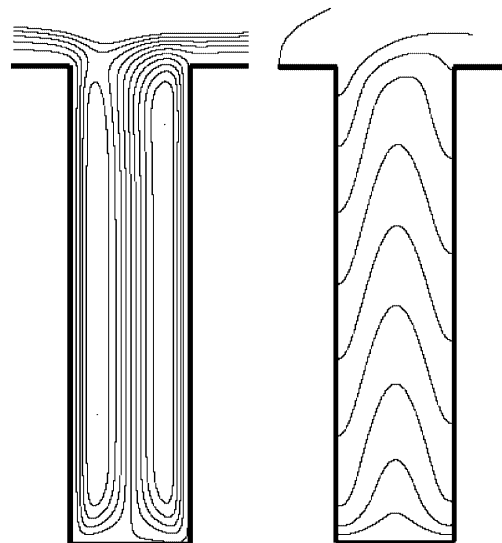


Fig. 1. Computed streamlines (left) and isopleths (right) for $\text{Pe}_w = 125$ and $A = h/w = 4$ and $w/\delta = 16$

like water having a density of 1000 kg/m^3 and a sound speed, c , of 1500 m/s .

Figure 1 illustrates the computed flow and transport within a feature having an aspect ratio of four and a Peclet number of 125. This choice corresponds to development of LIGA features having a width of $30 \text{ }\mu\text{m}$ at an acoustic power level of $I = 100 \text{ kW/m}^2$ (10 W/cm^2), assuming a polymer fragment diffusivity of $D = 10^{-11} \text{ m}^2/\text{s}$. Streamlines are shown on the left side of the figure. Isopleths, lines of constant fragment concentration, are shown on the right side. The flow within the feature is torroidal with downflows along the walls driven by large Reynolds stress gradients in the acoustic boundary layers. The upflow in the center is simply a consequence of continuity.

The flow along the midsection of the feature does not vary with elevation. With increasing aspect ratio, the flow along the midsection remains the same but extends over a larger fraction of the feature. The turning regions at the ends are not, however, affected by changes in the aspect ratio for aspect ratios greater than two or three. The asymmetry of the flow near the feature mouth results from applying a normalized shear stress of $\text{Pe}_w/4/\delta^*$ to the fluid above the feature to account for the formation of an acoustic boundary layer on the wafer face; this has a relatively minor influence on the fragment transport.

The isopleths on the right of Fig. 1 are swept downward by descending flow adjacent to the feature walls. Upward flow in the center is also apparent. The close spacing of the isopleths near the feature bottom is indicative of the large diffusion flux at the lower surface. Integration of this flux over the feature bottom yields the Sherwood number, representing the ratio of the vertical species transport compared to that which would have occurred by diffusion alone.

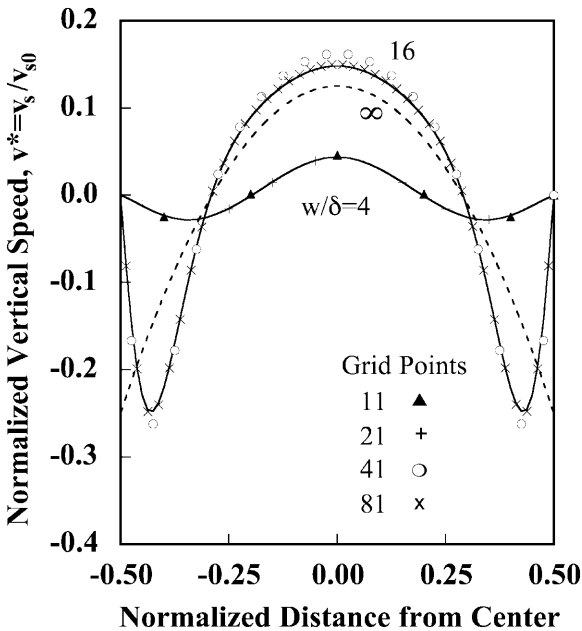


Fig. 2. Normalized streaming velocity along feature versus normalized distance from feature center. Solid lines are analytical solutions; symbols are numerical results. Dotted line is asymptotic solution for $w/\delta \gg 1$

$$\text{Sh} = \left(\frac{h}{D\Delta C} \right) \frac{1}{w} \int_0^w D \frac{\partial C}{\partial y} dx \quad (9)$$

The Sherwood number is 3.5 for the example in Fig. 1.

As seen in Fig. 2, streaming velocities computed numerically at the feature midheight (symbols) are in excellent agreement with exact analytical solutions that apply at all intermediate elevations when the aspect ratio is large [9]. The steady motion is severely suppressed when $w/\delta < 4$.

When the feature width greatly exceeds the acoustic boundary layer thickness ($w/\delta \gg 1$), the velocity profile approaches an asymptotic solution having a parabolic shape and a maximum downward speed of $v^* = v/u_{s0} = -0.25$ adjacent to the wall, as indicated by the dotted line in Fig. 2. Because the maximum speed is roughly coincident with the inner edge of the acoustic boundary layer at $x^* \sim \delta/w \ll 1$, the resulting velocity field is nearly equivalent to that driven by a slip velocity on the vertical walls. Thus, since $w/\delta > 50$ in the practical examples presented here, flow and transport can be accurately and efficiently calculated by applying a slip velocity of normalized magnitude $\text{Pe}_w/4$ rather than explicitly including the Reynolds stresses comprising F in Eq. (3).

5 Analytical transport model

The symbols in Fig. 3 illustrate the numerically computed variation of the reduced Sherwood number, Sh_1 , with a modified Peclet number, $\overline{\text{Pe}}$, based on the mean downflow speed \bar{V} .

$$\overline{\text{Pe}} = \frac{\bar{V}w}{D} = \text{Pe}_w \frac{\bar{V}}{u_{s0}} \sim \text{Pe}_w \frac{0.4}{4} \sim 0.1\text{Pe} \quad (10)$$

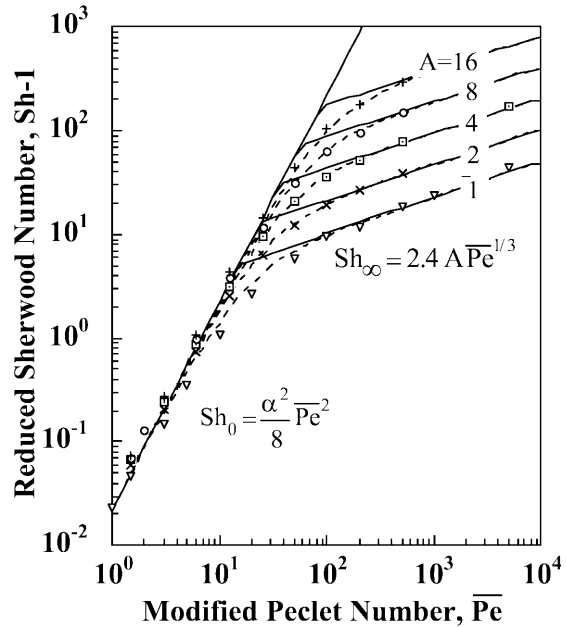


Fig. 3. Variation of Sherwood number with Peclet number. Solid lines are asymptotes, dotted line is composite formula; symbols are numerical calculations

The value 0.4 appearing here is obtained by integration of the parabolic velocity profile for $w \gg \delta$ across a trench-like feature; the corresponding value for a circular hole is 0.5. In either geometry, the maximum downflow speed adjacent to the wall is $V_{\max} = u_{s0}/4$ and the downflow region spans a fraction $\alpha \sim 0.42$ of the feature half-width.

When the Peclet number is relatively small, the numerical calculations (symbols) in Fig. 3 follow a single line given by

$$\text{Sh}_0 = \lim_{\text{Pe} \rightarrow 0} (\text{Sh} - 1) = \frac{\alpha^2}{8} \overline{\text{Pe}}^2 \quad (11)$$

In this regime the enhancement is independent of the aspect ratio, A . At high Peclet numbers, however, the calculations for each aspect ratio follow separate asymptotes of the form

$$\text{Sh}_\infty = \lim_{\text{Pe} \rightarrow \infty} (\text{Sh} - 1) \approx 2.4A\overline{\text{Pe}}^{1/3} \quad (12)$$

Each asymptote is indicated by a solid line in Fig. 3. These asymptotic expressions for small and large Peclet numbers may be combined to form a simple but accurate approximation

$$\text{Sh} = 1 + \frac{\text{Sh}_0 \text{Sh}_\infty}{\text{Sh}_0 + \text{Sh}_\infty} \quad (13)$$

shown by dotted lines in Fig. 3. The analytical approximation of Eq. (13) is seen to be in excellent agreement with the symbols representing numerical results. This composite formula remains valid so long as the acoustic boundary layer is thin compared to the feature width.

6 Coupled kinetics and transport

LIGA development rates are limited both by fragment transport rates and by surface dissolution kinetics. Previous studies of the kinetics have shown that the dissolution rate of PMMA in a GG developer fluid may be well approximated by the expression [10].

$$R = G \frac{(Q/B)^p}{1 + (Q/B)^p} e^{-\frac{E}{R}(\frac{1}{T} - \frac{1}{T_0})} \quad (14)$$

in which Q is the absorbed X-ray dose, E is the activation energy, T is the absolute temperature and T_0 is a reference temperature. The constants G , B , and p are chosen as 12.3 ($\mu\text{m}/\text{min}$), 8.44 kJ/cm^3 , and 3.81 to provide a best fit to the data reported by Pantenburg et al. [11] for $T = 21^\circ\text{C}$ and for doses that span the range used in the examples treated below. These values are somewhat different than those used by Tan et al. [10] to fit a data set that extends to higher doses. The activation energy is typically on the order of 140 kJ/mol , but this is of no importance to our examples as they are limited to cases with $T = T_0 = 21^\circ\text{C}$.

In a quasi-steady development process the recession rate, dh/dt , is proportional to the net dissolution rate, $R(\rho_s - \rho_1 C_b)$, which must be in balance with the rate of fragment transport from the development surface into the bath, $\rho_1 D \text{Sh} \Delta C/h$ [12].

$$\rho_s \frac{dh}{dt} = R(\rho_s - \rho_1 C_b) = \rho_1 \text{Sh} D \frac{\Delta C}{h} \quad (15)$$

Here, ρ_s and ρ_1 are the PMMA solid density and the fluid bulk density, respectively, and $\Delta C = C_b$ since the partial mass density at the feature bottom, C_b , is large compared to that in the bath. The second of the preceding equalities may be solved for $C^* = C_b \rho_1 / \rho_s$ to yield

$$\frac{dh}{dt} = R(1 - C^*) \quad \text{where } C^* = \frac{hR}{hR + D\text{Sh}} \quad (16)$$

7 Comparison with data

Predicted development histories are now compared with measurements made by Zanghellini et al. [3]. The absorbed dose profiles through the resist are computed using the LEXD code. These profiles are nearly exponential, but the deviations from exponential behavior can be important because of the very strong dependence of dissolution rate on absorbed dose. The top and bottom doses are of course identical to those reported by Zanghellini. The measured acoustic intensity is used to compute the modified Peclet number, $\overline{\text{Pe}}$, from Eqs. (7), (8) and (10). The variation of development depth is determined by numerical integration of Eq. (16a). For each time step, the instantaneous feature depth and local absorbed dose are used in calculating the nominal dissolution rate, R , and Sherwood number, Sh , from Eq. (14) and Eqs. (11–13), respectively. These values are then substituted into Eq. (16) to obtain C^* and the instantaneous recession rate, dh/dt , for the current time step.

Figure 4 compares our computed development histories for 30 μm features with measurements presented in Fig. 4 of Zanghellini's paper [3]. The PMMA fragment diffusivity, $D = 4.5 \times 10^{-12} \text{m}^2/\text{s}$, used in all three calculations was chosen to provide a good fit to the measured data for

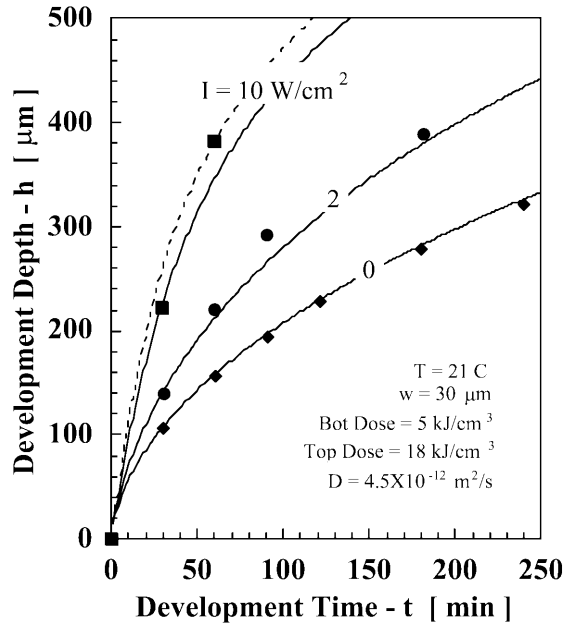


Fig. 4. Comparison of present analytical model (solid lines) with development histories (symbols) observed by Zanghellini et al. [3]. Dotted line indicates maximum kinetic-limited dissolution rate

development in the absence of sonic agitation ($I = 0$). This diffusivity, although quite small, appears consistent with available data for comparable molecular weights and fragment concentrations [13]. It is seen in Fig. 4 that the predicted increase in development depths for sonic agitation is in remarkably good agreement with Zanghellini's data.

For the strongest agitation shown in Fig. 4, 100 kW/m^2 (10 W/cm^2), the development rate is limited almost entirely by dissolution kinetics. Note, however, that there is no indication that acoustic agitation has altered the dissolution kinetics, since the observed rates do not exceed the maximum rates (dotted line) based on the Pantenburg data [11]. At 100 kW/m^2 (10 W/cm^2), the development rate decreases with depth mainly because of the reduction in the local absorbed dose. However, for $I = 20 \text{ kW/m}^2$ (2 W/cm^2) the transport in a $30 \text{ }\mu\text{m}$ hole is insufficient to maintain a low fragment concentration at the feature bottom. In this regime the development rate decreases with depth due to the increasing transport path length as well as reduced dose. Moreover, since transport is dependent on feature size, development depths also become sensitive to the feature size.

The computed variation of development depth with feature size is shown in Fig. 5 for various development times and for two agitation intensities; the dose profile is the same as that used in Fig. 4. Development depths are seen to increase strongly with feature size for holes smaller than about $150 \text{ }\mu\text{m}$. This is consistent with the variation of the acoustically driven fragment flux, f_a , with feature width that may be deduced from the low Peclet number asymptote of Eq. (11).

$$\lim_{\text{Pe} \rightarrow 0} f_a \propto \text{Sh} \frac{D}{h} \propto \text{Pe}^2 \frac{D}{h} \propto \frac{I^2 w^2}{Dh} \quad (17)$$

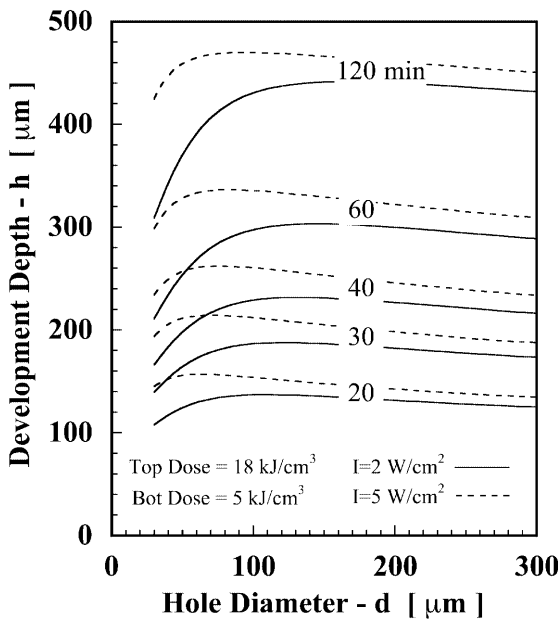


Fig. 5. Variation of computed development depth with hole size at various times. $T = 21 \text{ }^\circ\text{C}$. Absorbed doses and polymer fragment diffusivity are the same as those in Fig. 4

The development depth also appears to decrease weakly with feature size for holes larger than $150 \text{ }\mu\text{m}$. Since wider features have larger Peclet numbers, this behavior is consistent with the dependence deduced from the high Peclet number relation of Eq. (12).

$$\lim_{\text{Pe} \rightarrow \infty} f_a \propto \text{Sh} \frac{D}{h} \propto \text{Pe}^{1/3} A \frac{D}{h} \propto \frac{I^{1/3} D^{2/3}}{w^{2/3}} \quad (18)$$

This downward trend with feature size is only weakly apparent in Fig. 5 partly because kinetic limitations become more important in larger features where transport is relatively strong. Even a very moderate convective flow across the wafer face would offset this reduction of development rates with feature width. No experimental data has been included in our Fig. 5 because of apparent inconsistencies between the data in Figs. 4 and 5 of [3].

Figure 6 is equivalent to Fig. 5 except that the absorbed doses are about half as large and data from [3] is included. The agreement is very good. Also, because the kinetic-limited dissolution rate is substantially reduced, an agitation intensity of 20 kW/m^2 (2 W/cm^2) provides fragment transport that maintains a very low fragment concentration at the bottoms of all features. Under these conditions all features appear to develop at nearly the same rate.

Relative uniformity of development depths can, however, be somewhat misleading because differences in development time are inversely proportional to the development rate. For this reason, the differences in development times for $I = 2 \text{ W/cm}^2$ in Figs. 5 and 6 are nearly identical even though the development depths are dramatically less uniform in Fig. 5. Differences in time are important because these, together with the development rate, determine the sidewall taper and extent of undercutting adjacent to the substrate.

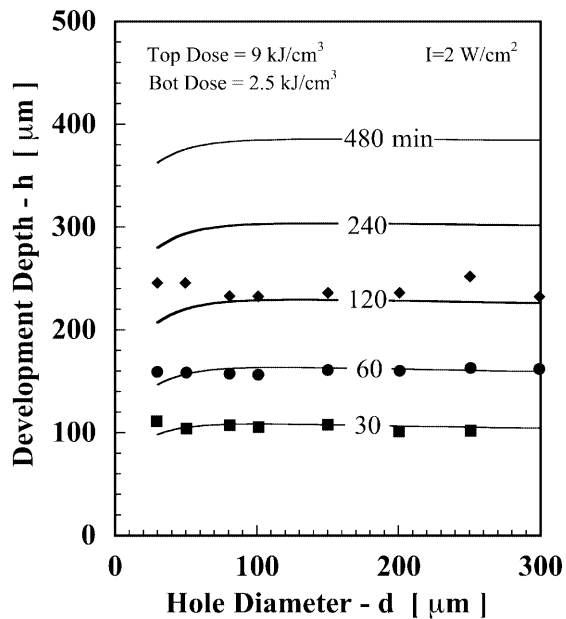


Fig. 6. Comparison of computed (lines) with measured (symbols) variation of development depth with hole size at various times. Absorbed dose is half that in Fig. 5

Summary and conclusions

The primary thesis of the present paper is that the observed enhancement of LIGA development rates by sonic agitation results from the induced acoustic streaming flow that circulates most of the fluid within high aspect-ratio features. In support of this hypothesis, polymer fragment transport along typical LIGA features was computed by numerically solving the Navier–Stokes equations together with a species transport equation accounting for fragment diffusion and advection. These numerical results were used to guide the derivation of an analytical model that yields transport rates in terms of process parameters.

LIGA development histories were computed by combining the preceding transport model with a semi-empirical model of PMMA dissolution kinetics. These calculations were found to be in good agreement with histories measured by Zanghellini et al. [3].

The analytical relationship presented here can be used to compute the variation in development times for the range of feature sizes on a wafer. As discussed in a complementary paper [12], differences in development times depends upon feature sizes, agitation intensity, diffusivity, and resist thickness, but are independent of absorbed dose profile and dissolution kinetics. Since allowable agitation intensities are limited by available hardware and by survival of fragile features, the minimum attainable difference in development times can be computed using the models explained here and in [12]. The allowable dose can then be chosen so that sidewall taper and undercutting near the substrate will be within acceptable limits.

References

1. Becker EW; Ehrfeld W; Hagemann P; Maner A; Munchmeyer D (1986) Fabrication of microstructures with high aspect

- ratios and great structural heights by synchrotron radiation lithography, galvanofarming and plastic moulding. *Micro-electronic Eng* 4: 35–56
2. Griffiths SK; Nilson RH; Bradshaw RW; Ting A; Bonivert W; Hachman JT; Hrubby JM (1998) Transport limitations in electrodeposition for LIGA microdevice fabrication. *Proceedings of the SPIE, Micromachining and Microfabrication Process Technology IV* 3511: 364–375
3. Zanghellini J; Achenbach S; El-Kholi A; Mohr J; Pantenburg FJ (1998) New development strategies for high aspect ratio microstructures. *Microsyst Technol* 4: 94–97
4. Lee KJ; Bucchignano J; Gelorme J; Viswanathan R (1997) Ultrasonic and dip resist development processes for 50 nm device fabrication. *J Vac Sci Technol B* 15(6): 2621–2626
5. Leighton TG (1994) *The Acoustic Bubble*. Academic Press, London
6. Busnaina AA; Kashkoush II; Gore GW (1995) An experimental study of megasonic cleaning of silicon wafers. *J Electrochem Soc* 142(8): 2812–2817
7. Rayleigh JWS (1945) *The Theory of Sound*. Dover, New York
8. Nyborg WL (1998) Acoustic streaming. In: Hamilton MF; Blackstock DT (eds), *Nonlinear Acoustics*, Chapter 7, Academic Press, London
9. Nilson RH; Griffiths SK (2000) Acoustic agitation for enhanced development of LIGA PMMA resists. *SPIE Proc. Micromachining and Microfabrication Process Technology VI*, 4174(5): 66–76
10. Tan MX; Bankert MA; Griffiths SK; Ting A; Boehme DR; Wilson S; Balsler LM (1998) PMMA dose studies at various synchrotron sources and exposure/development conditions. *SPIE Proceedings, Materials and Device Characterization in Micromachining* 3512: 262–270
11. Pantenburg FJ; Achenbach S; Mohr J (1998) Influence of developer temperature and resist material on the structure quality in deep X-Ray lithography. *J Vac Sci Tech B* 16: 3547–3551
12. Griffiths SK; Nilson RH (2002) Transport limitations on development times of LIGA PMMA resists. *Microsyst Technol* 8: 335–342
13. Tirrell M (1984) Polymer self-diffusion in entangled systems. *Rubber Chem Technol* 57(3): 523–554